The lateral meningocele syndrome mutation causes marked osteopenia in mice

Received for publication, May 30, 2018, and in revised form, July 11, 2018 Published, Papers in Press, July 24, 2018, DOI 10.1074/jbc.RA118.004242

Ernesto Canalis[‡§¶1], Jungeun Yu[‡¶], Lauren Schilling[‡¶], Siu-Pok Yee[‖], and Stefano Zanotti[‡§¶2]**

*From the Departments of [‡]Orthopaedic Surgery, [§]Medicine, and [‖]Cell Biology, [¶]UConn Musculoskeletal Institute, and **Center for Mouse Genome Modification, UConn Health, Farmington, Connecticut 06030*

Edited by Jeffrey E. Pessin

Lateral meningocele syndrome (LMS) is a rare genetic disorder characterized by neurological complications and osteoporosis. LMS is associated with mutations in exon 33 of *NOTCH3* leading to a truncated protein lacking sequences for NOTCH3 degradation and presumably causing NOTCH3 gain of function. To create a mouse model reproducing human LMS-associated mutations, we utilized CRISPR/Cas9 to introduce a tandem termination codon at bases 6691–6696 (ACCAAG→TAATGA) and verified this mutation (*Notch3*$^{tm1.1Ecan}$) by DNA sequencing of F1 mice. One-month-old male and female heterozygous *Notch3*$^{tm1.1Ecan}$ mice had cancellous and cortical bone osteopenia but exhibited no obvious neurological alterations, and histopathology of multiple organs revealed no abnormalities. Microcomputed tomography of these mutants revealed a 35–60% decrease in cancellous bone volume associated with a reduction in trabecular number and decreased connectivity. During maturation, cancellous and cortical bones were restored in female but not in male mice, which exhibited cancellous bone osteopenia at 4 months. Cancellous bone histomorphometry revealed increased osteoblast and osteocyte numbers and a modest increase in osteoclast surface and bone formation rate. *Notch3*$^{tm1.1Ecan}$ calvarial osteoblasts had increased proliferation and increased bone γ-carboxyglutamate protein (*Bglap*) and TNF superfamily member 11 (*Tnfsf11*) mRNA levels and lower *Tnfrsf11b* levels. *Tnfsf11* mRNA was increased in osteocyte-rich femora from *Notch3*$^{tm1.1Ecan}$ mice. Cultures of bone marrow–derived macrophages from *Notch3*$^{tm1.1Ecan}$ mice revealed increased osteoclast formation, particularly in cocultures with osteoblasts from *Notch3*$^{tm1.1Ecan}$ mice. In conclusion, the *Notch3*$^{tm1.1Ecan}$ mutation causes osteopenia despite an increase in osteoblast proliferation and function and is associated with enhanced *Tnfsf11* expression in osteoblasts and osteocytes.

Notch1–4 are transmembrane receptors that mediate communication between neighboring cells and play a fundamental role in cell fate decisions (1, 2). The Notch extracellular domain interacts with classic ligands of the Jagged and Delta-like families (3) (Fig. 1). The negative regulatory region is the site of cleavage required for Notch activation, and it is located at the junction of the extracellular and the transmembrane domains of Notch. Following the activation of Notch, its Notch intracellular domain (NICD)[3] is released and translocates to the nucleus (4, 5). There the NICD, recombination signal–binding protein for Ig of κ region (RBPJκ), and mastermind-like form a complex that leads to the induction of target gene transcription (2, 6, 7). Gene targets of this canonical Notch signaling are hairy and enhancer of split (*Hes*) and HES-related with YRPW motif (*Hey*) (8–10). A proline (P)-, glutamic acid (E)-, serine (S)-, threonine (T)-rich motif (PEST) domain is located in the C terminus of Notch, and ubiquitin ligases target this domain for the degradation of the NICD (11, 12) (see Fig. 1).

Notch1, -2, and -3 and low levels of Notch4 are expressed in skeletal cells (13, 14). Although some functional overlap is possible between Notch receptors, each Notch receptor exhibits unique roles in physiology (15–17). Differences in the actions of Notch receptors relate to differences in their structure, cellular and temporal expression, and highly specific negative regulatory region domains and variations in the interactions of specific NICDs with RBPJκ (18, 19). Notch1 and Notch2 have been studied extensively for their role in skeletal homeostasis (13, 20–25). Notch1 inhibits osteoblast and osteoclast differentiation, whereas Notch2 inhibits osteoblastogenesis but induces osteoclastogenesis, confirming distinct effects of the various Notch receptors in skeletal cells (13, 20, 26). Notch3 has a distinct structure, and its NICD is different from that of Notch1 and -2, indicating a potentially unique physiological role for Notch3 (27). However, knowledge regarding the actions of Notch3 in the skeleton is limited.

Lateral meningocele syndrome (LMS) or Lehman syndrome (Online Mendelian Inheritance in Man 130720) is a rare gen-

This work was supported by NIAMS Grants AR063049 and AR072987 and NIDDK Grant DK045227 from the National Institutes of Health (all to E. C.). The authors declare that they have no conflicts of interest with the contents of this article. The content is solely the responsibility of the authors and does not necessarily represent the official views of the National Institutes of Health.
This article was selected as one of our Editors' Picks.
This article contains Fig. S1.

[1] To whom correspondence should be addressed: Dept. of Orthopaedic Surgery, UConn Health, Farmington, CT 06030-5456. Tel.: 860-679-7978; Fax: 860-679-1474; E-mail: canalis@uchc.edu.
[2] Present address: Rare Diseases, Sanofi, Framingham, MA 01701.

[3] The abbreviations used are: NICD, Notch intracellular domain; α-MEM, α-minimum essential medium; BMM, bone marrow–derived macrophage; FBS, fetal bovine serum; *Hes*, hairy and enhancer of split; *Hey*, HES-related with YRPW motif; LMS, lateral meningocele syndrome; M-CSF, macrophage colony-stimulating factor; μCT, microcomputed tomography; MTT, 3-[4,5-dimethylthiazol-2-yl]-2,5-diphenyltetrazolium bromide; PTH, parathyroid hormone; qRT-PCR, quantitative RT-PCR; RANKL, receptor activator of NF-κB ligand; RBPJκ, recombination signal–binding protein for Ig of κ region; sg, single guide; TRAP, tartrate-resistant acid phosphatase; *Tnfsf11*, tumor necrosis factor superfamily member 11; *Tnfrsf11b*, tumor necrosis factor receptor superfamily 11b; *Bglap*, γ-carboxyglutamate protein; sg, single guide; ANOVA, analysis of variance.

etic disorder that presents with neuromuscular dysfunction, meningoceles, and distinct facial features (28). The clinical features of LMS include developmental delay, decreased muscle mass, and cardiac valve defects. Skeletal abnormalities are frequent, including thickening of the calvarial vault, craniofacial defects, short stature, scoliosis, and bone loss (29, 30). Exome-wide sequencing of individuals affected by LMS demonstrated the presence of mutations in exon 33 of *NOTCH3*. These mutations create a stop codon so that the PEST domain is not translated (31). Because the PEST domain is necessary for the ubiquitination and degradation of NOTCH3, the NOTCH3 NICD is presumably stable, resulting in persistent signaling and gain of function.

Despite the skeletal manifestations reported in LMS, there is limited knowledge about the mechanisms that operate or the actions of NOTCH3 in the skeleton. The purpose of the present work was to provide an understanding of the skeletal manifestations of LMS and responsible mechanisms. For this purpose, a mouse (*Notch3*$^{tm1.1Ecan}$) model reproducing the *NOTCH3* mutation harbored by subjects affected by LMS was engineered. To create an LMS mutant mouse, we introduced a tandem termination codon, ACCAAG→TAATGA, into exon 33 of the *Notch3* gene at bp 6691–6696 from the start of translation. In the present work, we report the skeletal phenotype and underlying mechanisms of *Notch3*$^{tm1.1Ecan}$ mice.

Results

Generation and general appearance of Notch3$^{tm1.1Ecan}$ *mutant mice*

The RNA-guided clustered regularly interspaced short palindromic repeat (CRISPR)-associated Cas9 nuclease system was used to target exon 33 of *Notch3* and introduce a TAATGA tandem termination codon at positions 6691–6696 from the start of translation (32–34). This genetic intervention leads to the translation of the truncated NOTCH3 protein T2231X consisting of 2230 amino acids (*versus* 2318 in WT). Single guide (sg) RNA, designed to cleave between nucleotides 6691 and 6692 of *Notch3*, and a single-strand DNA containing the tandem stop codon TAATGA were coinjected into C57BL/6J one-cell embryos with *Cas9* mRNA (Fig. 1). The proper insertion of the *Notch3* 6691–6696 ACCAAG→TAATGA mutation was confirmed by DNA sequencing of F1 mice (Fig. 1). Heterozygous mutant mice were compared with sex-matched WT littermates in a C57BL/6J genetic background. Breeding between heterozygous LMS mutant and WT mice yielded offsprings composed of 55% WT and 45% heterozygous *Notch3*$^{tm1.1Ecan}$ mice. *Notch3*$^{tm1.1Ecan}$ mice appeared healthy, did not exhibit overt neuromuscular signs, and were fertile. Percent body fat, fasting serum insulin and glucose levels, and serum 17β-estradiol and parathyroid hormone (PTH) levels were not different between *Notch3*$^{tm1.1Ecan}$ and controls (Table 1). One-month-old heterozygous *Notch3*$^{tm1.1Ecan}$ mice did not appear different from controls and had a weight that was ~10% lower than controls. However, the difference in weight was less pronounced as the mice matured, and at 4 months of age *Notch3*$^{tm1.1Ecan}$ mice weighed ~5% less than control littermates. Femoral length was slightly shorter in *Notch3*$^{tm1.1Ecan}$ mice at 1 month but not at 4 months of age when femoral length was not different from controls (Fig. S1).

Femoral microarchitecture of Notch3$^{tm1.1Ecan}$ *mutant mice*

Microcomputed tomography (μCT) of the distal femur demonstrated that 1-month-old male and female *Notch3*$^{tm1.1Ecan}$ mutant mice had a 35–60% decrease in cancellous bone volume (Table 2 and Figs. 2 and 3). The decreased cancellous bone was associated with decreased trabecular number and connectivity and higher structure model index, indicating a predominance of rodlike trabeculae. Trabecular thickness was not affected. Cortical bone was thin and porous in 1-month-old *Notch3*$^{tm1.1Ecan}$ mutant mice of both sexes, although total bone area was not different from controls, indicating normal bone size (Table 2 and Figs. 2 and 3). The decrease in trabecular bone volume was sustained and observed in 4-month-old male, but not female, *Notch3*$^{tm1.1Ecan}$ mutant mice. Male mice had a significant decrease in cancellous bone volume of ~30% associated with decreased trabecular number and connectivity. However, cortical bone was not altered in *Notch3*$^{tm1.1Ecan}$ mice of either sex (Table 2).

Femoral histomorphometry of Notch3$^{tm1.1Ecan}$ *mutant mice*

In accordance with the μCT findings, cancellous bone histomorphometry of femora from *Notch3*$^{tm1.1Ecan}$ mice of both sexes revealed decreased bone volume/tissue volume and trabecular number (Table 3 and Fig. 3). There was an ~2-fold increase in the number of osteoblasts and in osteoblast surface/bone surface in *Notch3*$^{tm1.1Ecan}$ mutant mice of both sexes as well as a 13–33% increase in osteocyte cell density. The higher osteoblast number was associated with an increase in mineral apposition rate in male *Notch3*$^{tm1.1Ecan}$ mutant mice and a nonsignificant (1.8–2.1-fold) increase in bone formation rate. Osteoclast surface/bone surface was increased in male *Notch3*$^{tm1.1Ecan}$ mutant mice, but osteoclast number/bone perimeter was not affected significantly in either sex. At 4 months of age, the cellular phenotype in male mutant mice was sustained, and they exhibited decreased bone volume/tissue volume associated with a 60% increase in osteoblast number and elevated bone formation rate when compared with WT sex-matched littermate mice (Table 4). However, neither osteoclast surface nor osteoclast number was significantly affected in *Notch3*$^{tm1.1Ecan}$ mice. These results suggest that *Notch3*$^{tm1.1Ecan}$ mice have a higher number of osteoblasts, possibly as a manifestation of high bone remodeling, but the cells are not sufficiently active to maintain skeletal homeostasis.

Gene expression in Notch3$^{tm1.1Ecan}$ *mutant mice*

To search for mechanisms that could operate in *Notch3*$^{tm1.1Ecan}$ mutants, tibiae were analyzed for changes in gene expression. Quantitative RT-PCR (qRT-PCR) revealed expression of *Notch3*$^{6691\text{-}TAATGA}$ transcripts and increased *Hey1*, *Hey2*, and *HeyL* mRNA levels in tibiae from mutant mice, demonstrating that Notch signaling was activated in bone (Fig. 4). In agreement with the increase in osteoclast surface in mutant mice, the expression of *Tnfsf11* mRNA, encoding for receptor activator

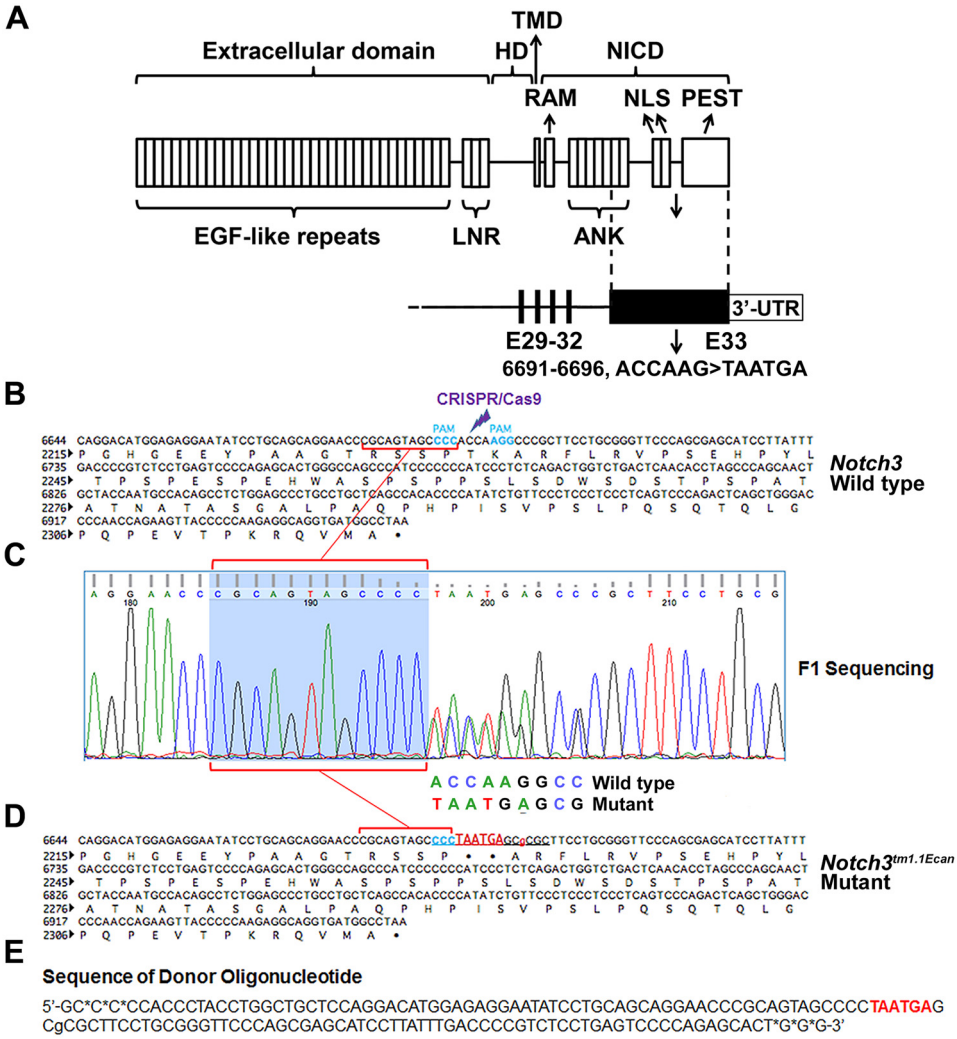

Figure 1. Domains of *Notch3* and engineering of the *Notch3*$^{tm1.1Ecan}$ mutant allele. *A*, domains of the Notch3 receptor depicting the 1) extracellular domain containing multiple epidermal growth factor (EGF)-like tandem repeats upstream of Lin12-Notch repeats (LNR); 2) heterodimerization domain (HD) that, in association with the Lin12-Notch repeats, forms the negative regulatory region; 3) transmembrane domain (TMD); and 4) NICD consisting of an RBPJκ-association module (RAM) linked to ankyrin (ANK) repeats and a nuclear localization sequence (NLS) upstream of a PEST domain. Under the NOTCH3 protein domains, the genomic structure of mutant exon 33 aligned with the corresponding protein structure is shown. *Black bars* represent exons (*E*) 29–32, the *black box* represents exon 33 containing the 6691–6696 ACCAAG→TAATGA mutation leading to a T2231X change at the amino acid level, and the *white box* represents the 3′-UTR. *B*, WT *Notch3* exon 33 sequence with protospacer adjacent motif (PAM) for CRISPR/Cas9 targeting. *C* and *D*, genomic DNA from ear samples of F1 pups was used as a template for PCR, and products were sequenced by the Sanger method. Sequencing of the DNA fragment spanning the *Notch3*$^{6691\text{-}TAATGA}$ mutation is shown in *C*. The 1:1 signal ratio for ACCAAG→TAATGA demonstrates heterozygosity for the mutation. The sequence of the mutant *Notch3*$^{tm1.1Ecan}$ allele is in *D*. *E*, sequence of donor oligonucleotide used to generate the *Notch3*$^{6691\text{-}TAATGA}$ mutant, including a downstream c→g mutation to ensure the mutation was not a random event. * represents phosphorothioate linkage to protect from exonuclease degradation.

Table 1

Percent body fat and hormonal/metabolic parameters in 4-month-old *Notch3*$^{tm1.1Ecan}$ mutant male and female mice and sex-matched control littermates

Body fat was determined by total body densitometry, and glucose and hormone levels were measured in fasting serum samples from *Notch3*$^{tm1.1Ecan}$ mutant mice and sex-matched control littermates. Values are means ± S.D.; $n = 3–4$. 17βE_2, 17β-estradiol.

	Males		Females	
	Control	*Notch3*$^{tm1.1Ecan}$	Control	*Notch3*$^{tm1.1Ecan}$
Body fat (%)	17.9 ± 0.8	17.6 ± 0.6	20.0 ± 0.4	21.5 ± 0.7
Glucose (mg/dl)	88 ± 2	84 ± 1	91 ± 2	86 ± 2
Insulin (μIU/ml)	114 ± 7	132 ± 6	120 ± 36	110 ± 20
PTH (pg/ml)	426 ± 65	322 ± 107	325 ± 89	294 ± 82
17βE_2 (pg/ml)			37 ± 4	42 ± 8

of NF-κB ligand (RANKL), was increased in femora from *Notch3*$^{tm1.1Ecan}$ mutant mice. A modest increase in *Tnfrsf11b* mRNA, encoding for osteoprotegerin, was noted.

Calvarial osteoblast cultures

To pursue the consequences of the *Notch3*$^{tm1.1Ecan}$ mutation in skeletal cells, calvarial osteoblasts were cultured. Osteoblasts from *Notch3*$^{tm1.1Ecan}$ mice, but not from controls, expressed *Notch3*$^{6691\text{-}TAATGA}$ transcripts. *Hey1* was transiently increased in *Notch3*$^{tm1.1Ecan}$ osteoblasts, whereas *HeyL* was increased for a 3-week culture period, documenting sustained activation of Notch signaling (Fig. 5). Osteoblast cultures from *Notch3*$^{tm1.1Ecan}$ mice expressed higher levels of *Bglap* (encoding for osteocalcin) and *Tnfsf11* mRNAs and lower levels of *Tnfrsf11b* mRNA than control cultures. To estimate the rate of cellular proliferation, the reduction of 3-[4,5-dimethylthiazol-2-yl]-2,5-diphenyltetrazolium bromide (MTT) to its formazan salt was measured during the initial phases of the culture. This "MTT assay" measures mitochondrial activity of cells and

Table 2

Femoral microarchitecture assessed by μCT of 1- and 4-month-old *Notch3*$^{tm1.1Ecan}$ mutant male and female sex-matched mice and control littermates

μCT was performed in distal femora for trabecular bone and midshaft for cortical bone from 1- and 4-month-old male and female *Notch3*$^{tm1.1Ecan}$ mutant mice and sex-matched control littermates. Values are means ± S.D. *, significantly different between control and *Notch3*$^{tm1.1Ecan}$, $p < 0.05$ by unpaired *t* test.

Males	1 Month		4 Month	
	Control n = 7	*Notch3*$^{tm1.1Ecan}$ n = 7	Control n = 11	*Notch3*$^{tm1.1Ecan}$ n = 10
Distal Femur Trabecular Bone				
Bone Volume/Total Volume (%)	7.4 ± 1.3	4.9 ± 1.3*	8.6 ± 2.4	6.3 ± 2.7*
Trabecular Separation (μm)	191 ± 16	244 ± 31*	217 ± 9	283 ± 23*
Trabecular Number (1/mm)	5.3 ± 0.5	4.2 ± 0.5*	4.6 ± 0.2	3.6 ± 0.3*
Trabecular Thickness (μm)	28 ± 2	26 ± 3	38 ± 6	41 ± 7
Connectivity Density (1/mm^3)	362 ± 124	201 ± 108*	173 ± 51	106 ± 51*
Structure Model Index	2.7 ± 0.1	3.0 ± 0.2*	2.4 ± 0.3	2.6 ± 0.3
Density of Material (mg HA/cm^3)	796 ± 40	781 ± 31	940 ± 87	969 ± 67
Femoral Midshaft Cortical Bone				
Bone Volume/Total Volume (%)	84.4 ± 1.5	81.3 ± 1.6*	89.1 ± 0.7	88.0 ± 1.5
Porosity (%)	15.6 ± 1.5	18.7 ± 1.6*	10.9 ± 0.7	12.0 ± 1.5
Cortical Thickness (μm)	103 ± 10	87 ± 6*	167 ± 8	158 ± 13
Total Area (mm^2)	1.7 ± 0.1	1.7 ± 0.1	1.8 ± 0.3	1.7 ± 0.1
Bone Area (mm^2)	0.57 ± 0.05	0.51 ± 0.02*	0.84 ± 0.08	0.81 ± 0.08
Periosteal Perimeter (mm)	4.7 ± 0.1	4.7 ± 0.1	4.7 ± 0.4	4.7 ± 0.2
Endocortical Perimeter (mm)	3.8 ± 0.1	3.9 ± 0.1*	3.4 ± 0.4	3.4 ± 0.2
Density of Material (mg HA/cm^3)	994 ± 17	974 ± 13*	1216 ± 33	1226 ± 32

Females	1 Month		4 Month	
	Control n = 4	*Notch3*$^{tm1.1Ecan}$ n = 4	Control n = 8	*Notch3*$^{tm1.1Ecan}$ n = 8
Distal Femur Trabecular Bone				
Bone Volume/Total Volume (%)	5.4 ± 1.0	2.2 ± 0.4*	4.7 ± 1.8	5.6 ± 1.3
Trabecular Separation (μm)	225 ± 21	360 ± 19*	305 ± 24	290 ± 21
Trabecular Number (1/mm)	4.5 ± 0.4	2.8 ± 0.1*	3.3 ± 0.3	3.5 ± 0.3
Trabecular Thickness (μm)	28 ± 3	24 ± 4	41 ± 6	40 ± 4
Connectivity Density (1/mm^3)	207 ± 74	64 ± 8*	70 ± 38	99 ± 30
Structure Model Index	3.0 ± 0.2	3.2 ± 0.1	3.0 ± 0.4	2.8 ± 0.2
Density of Material (mg HA/cm^3)	768 ± 12	739 ± 14*	924 ± 62	945 ± 86
Femoral Midshaft Cortical Bone				
Bone Volume/Total Volume (%)	84.3 ± 0.6	80.2 ± 0.7*	88.5 ± 0.5	88.6 ± 1.0
Porosity (%)	15.7 ± 0.6	19.9 ± 0.7*	11.5 ± 0.5	11.4 ± 1.0
Cortical Thickness (μm)	102 ± 6	83 ± 3*	169 ± 6	166 ± 7
Total Area (mm^2)	1.5 ± 0.1	1.6 ± 0.2	1.6 ± 0.1	1.5 ± 0.1
Bone Area (mm^2)	0.51 ± 0.06	0.46 ± 0.05	0.78 ± 0.04	0.77 ± 0.03
Periosteal Perimeter (mm)	4.4 ± 0.2	4.4 ± 0.3	4.4 ± 0.1	4.4 ± 0.1
Endocortical Perimeter (mm)	3.6 ± 0.2	3.7 ± 0.2	3.1 ± 0.1	3.1 ± 0.1
Density of Material (mg HA/cm^3)	998 ± 9	964 ± 9*	1239 ± 35	1229 ± 44

as such is a proxy for cell proliferation. Osteoblasts from *Notch3*$^{tm1.1Ecan}$ mice proliferated at a rate 1.5 higher than that of cells from WT controls, an effect that is consistent with the increased number of osteoblasts in *Notch3*$^{tm1.1Ecan}$ mutants *in vivo* (Fig. 5). The results indicate enhanced osteoblast proliferation and differentiation in cells from *Notch3*$^{tm1.1Ecan}$ mutants as well as an increased ratio of RANKL to osteoprotegerin, providing a possible explanation for the findings *in vivo*.

Osteocyte-enriched cultures

Because a possible explanation for the *Notch3*$^{tm1.1Ecan}$ phenotype was an increase in osteoclastogenesis and because osteocytes play a major role in the control of bone resorption, we examined the expression of *Tnfsf11* mRNA in enzymatically/EDTA-digested osteocyte-rich femora (14, 35). Osteocytes expressed the *Notch3*$^{6691\text{-}TAATGA}$ transcript and increased levels of *Hey1*, *Hey2*, and *HeyL*, indicating enhanced Notch signaling. *Tnfsf11* mRNA was increased 1.6-fold in osteocytes from *Notch3*$^{tm1.1Ecan}$ mutant mice, whereas the expression of *Tnfrsf11b* was not affected (Fig. 6).

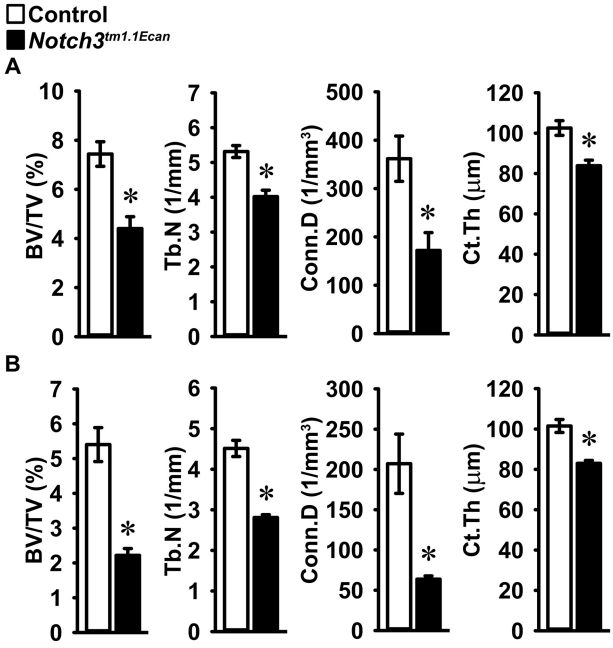

Figure 2. Femoral architecture assessed by μCT of distal femora from 1-month-old male (*A*) and female (*B*) *Notch3*$^{tm1.1Ecan}$ mutant (*black bars*) and control littermates (*white bars*) mice. Data are expressed as cancellous bone volume/total volume (*BV/TV*), trabecular number (*Tb.N*), connectivity density (*Conn.D*), and cortical bone thickness (*Ct.Th*). Values are expressed as means ± S.D. (*error bars*); number of observations for *Notch3*$^{tm1.1Ecan}$ and control males, $n = 7$ each, and *Notch3*$^{tm1.1Ecan}$ and control females, $n = 4$ each. *, significantly different between *Notch3*$^{tm1.1Ecan}$ mutant and WT controls, $p < 0.05$ by unpaired *t* test.

In vitro osteoclast formation

To explore whether a direct effect on osteoclast differentiation was operational, bone marrow–derived macrophages (BMMs) were isolated from *Notch3*$^{tm1.1Ecan}$ mutants and littermate controls. BMMs were cultured in the presence of macrophage colony-stimulating factor (M-CSF) at 30 ng/ml for 3 days and subsequently in the presence of M-CSF (30 ng/ml) and RANKL at 10 ng/ml. The number of tartrate-resistant acid phosphatase (TRAP)-positive multinucleated cells was increased in cultures from *Notch3*$^{tm1.1Ecan}$ mutants (Fig. 7). However, *Notch3*$^{tm1.1Ecan}$ mutant BMMs did not express *Notch3*$^{6691\text{-}TAATGA}$ transcripts, and neither mutant nor WT cells expressed detectable levels of *Notch3* mRNA. The results indicate that even though *Notch3*$^{tm1.1Ecan}$ mutant cells exhibited enhanced osteoclast differentiation the cellular phenotype is likely secondary to events that occurred *in vivo* prior to cell isolation, such as exposure to increased levels of RANKL. To determine whether the osteoblast or osteoclast was responsible for the enhanced osteoclastogenesis, BMMs from control and *Notch3*$^{tm1.1Ecan}$ mice were cocultured with osteoblasts from the respective mouse lines. Osteoclast differentiation was increased in BMMs from *Notch3*$^{tm1.1Ecan}$ mutants whether they were cultured in the presence of WT or mutant osteoblasts. In addition, osteoblasts from *Notch3*$^{tm1.1Ecan}$ mice enhanced osteoclastogenesis in both WT and *Notch3*$^{tm1.1Ecan}$ mutant BMMs. The results demonstrate both a BMM- and an osteoblast-dependent effect as responsible for the increased osteoclast differentiation in *Notch3*$^{tm1.1Ecan}$ mutants.

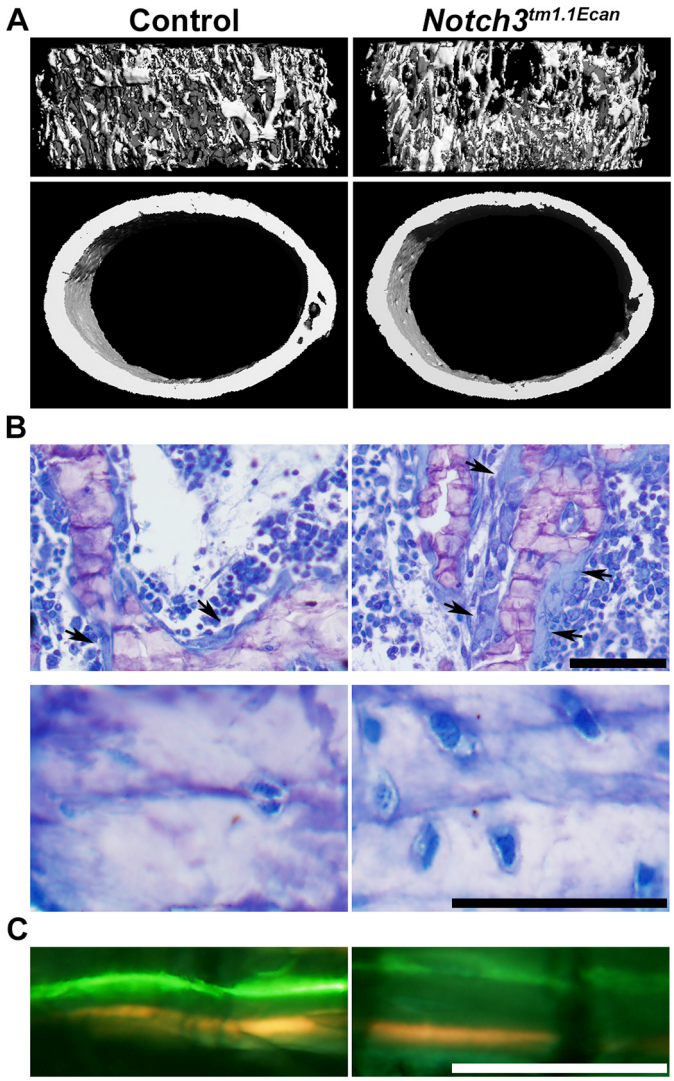

Figure 3. *A*, representative microcomputed tomography images of proximal trabecular bone and midshaft of femora showing cancellous bone osteopenia and decreased trabecular number and thinner cortical bone in *Notch3*$^{tm1.1Ecan}$ mutant mice. The complete data set is shown in Table 2. *B*, representative static cancellous bone histological sections stained with toluidine blue showing increased number of osteoblasts (*arrows*) (*B*, *upper panels*) and osteocytes (*B*, *lower panels*) in *Notch3*$^{tm1.1Ecan}$ mice. *C*, calcein and demeclocycline labeling of cancellous bone showing a higher mineral apposition rate in *Notch3*$^{tm1.1Ecan}$ mice compared with control. The complete data set is shown in Table 3. All representative images are from femora from 1-month-old male *Notch3*$^{tm1.1Ecan}$ mutant and sex- and age-matched littermate WT controls. *Scale bars*, 50 μm.

Discussion

The present work indicates that mice harboring a *Notch3* gain-of-function mutation exhibit bone loss that affects both the cancellous and cortical compartments. The osteopenia was detected in 1-month-old mice of both sexes, although in mature animals the osteopenic phenotype affected the cancellous bone of male, but not female, mutant mice. The abatement of the osteopenia in mature female mice might have been related to a decrease in bone remodeling, secondary to an effect of estrogens on the skeleton. Estrogens decrease the lifespan of osteoclasts by promoting their apoptosis and suppress the secretion of the cytokine IL-7 by osteoblasts with a consequent decrease in RANKL expression and osteoclastogenesis (36–38). The phenotype of the *Notch3*$^{tm1.1Ecan}$ mutant mouse is congruent with the bone loss observed in humans with LMS. However, there is no information on sex- or age-related changes in bone mass in subjects affected by LMS because the number of cases reported is small (29, 31). *Notch3*$^{tm1.1Ecan}$ mutant mice did not have obvious neurological manifestations reported in humans afflicted by the disease. Moreover, histopathology of brain, lungs, heart, liver, spleen, and kidneys did not reveal any obvious abnormalities in *Notch3*$^{tm1.1Ecan}$ mice.[4] A limitation of the present work is that relatively young mice were studied, and the phenotype might evolve as the mice age.

Stabilization of NOTCH3 protein is probably responsible for the increased Notch3 activity. The mutation in *Notch3*$^{tm1.1Ecan}$ mice was introduced upstream of the PEST domain, and this domain is essential for the ubiquitination of NOTCH3 (39). Similarly, mutations in exon 34 upstream of the PEST domain of *Notch1* or *Notch2* result in Notch gain of function and enhanced Notch signaling (40–42). The mechanism in LMS is analogous to that found in Hajdu–Cheney syndrome where affected individuals harbor mutations in exon 34 of *NOTCH2* (43–45). The inheritance of LMS is not established, and autosomal-dominant inheritance as well as *de novo* heterozygous truncating mutations in exon 33 of *NOTCH3* has been reported (29).

The osteopenia of *Notch3*$^{tm1.1Ecan}$ mutants was associated with an increase in the number of osteoblasts secondary to enhanced cell replication. Although bone formation was increased, the enhanced osteoblast number and function were not sufficient to maintain skeletal homeostasis, so bone loss occurred. *In vitro* cultures of osteoblasts revealed increased *Bglap* expression in *Notch3*$^{tm1.1Ecan}$ cells, indicating that osteoblast maturation was not impaired. There was a 45% increase in osteoclast surface/bone surface. This finding indicates that an increase in bone resorption contributed to the phenotype. This was secondary to an increased expression of RANKL and suppressed osteoprotegerin in cells of the osteoblast lineage. The capacity of osteoclast precursors to differentiate into mature osteoclasts in response to RANKL was enhanced in *Notch3*$^{tm1.1Ecan}$ mutants, although cells of the myeloid lineage do not express either WT or mutant *Notch3* transcripts. This suggests that the enhanced osteoclastogenesis *in vitro* reflected events occurring *in vivo*. Cocultures of BMMs with osteoblasts confirmed that the osteoblast of *Notch3*$^{tm1.1Ecan}$ mutants contributed to the enhanced osteoclastogenesis, an effect congruent with the increased expression of RANKL by the osteoblast. There was a greater number of osteocytes in cancellous bone of *Notch3*$^{tm1.1Ecan}$ mice, and this is probably secondary to the increased number of osteoblasts. Osteocytes are an important source of RANKL and likely contributed to the osteopenic phenotype observed (46–49).

The phenotype reported in *Notch3*$^{tm1.1Ecan}$ mutant mice is different from that observed in Notch1 NICD– expressing mice or that reported in mice harboring a *Notch2* gain-of-function mutation replicating Hajdu–Cheney syndrome (26). Notch1 activation in undifferentiated osteoblasts precludes their mat-

[4] E. Canalis, unpublished observations.

Table 3

Cancellous bone histomorphometry of 1-month-old *Notch3*$^{tm1.1Ecan}$ mutant male and female mice and sex-matched control littermates

Histomorphometry was carried out on sagittal sections of distal femora from 1-month-old male and female *Notch3*$^{tm1.1Ecan}$ mutant mice and sex-matched control littermates. Values are means ± S.D.

	Males		Females	
	Control ($n = 6$)	*Notch3*$^{tm1.1Ecan}$ ($n = 6$)	Control ($n = 7$)	*Notch3*$^{tm1.1Ecan}$ ($n = 7$)
Static histomorphometry				
Bone volume/tissue volume (%)	14.2 ± 3.1	9.8 ± 2.6[a]	10.3 ± 1.5	7.5 ± 2.3[a]
Trabecular separation (μm)	226 ± 48	307 ± 66[a]	268 ± 40	427 ± 182[a]
Trabecular number (1/mm)	3.9 ± 0.7	3.0 ± 0.5[a]	3.4 ± 0.6	2.4 ± 0.7[a]
Trabecular thickness (μm)	36.0 ± 3.4	32.1 ± 6.1	30.4 ± 2.8	31.0 ± 4.8
Osteoblast surface/bone surface (%)	10.5 ± 6.8	25.4 ± 7.6[a]	12.1 ± 6.2	21.6 ± 7.7[a]
Osteoblasts/bone perimeter (1/mm)	10.3 ± 6.6	24.5 ± 7.2[a]	11.9 ± 5.9	20.3 ± 6.6[a]
Osteoid surface/bone surface (%)	1.2 ± 1.4	3.5 ± 2.4	1.0 ± 0.9	2.4 ± 1.6
Osteocytes (mm^2)	565 ± 46	751 ± 151[a]	628 ± 29	710 ± 84[a]
Osteoclast surface/bone surface (%)	13.9 ± 5.9	20.3 ± 4.2[b]	20.5 ± 3.3	23.7 ± 4.1
Osteoclasts/bone perimeter (1/mm)	6.6 ± 1.4	8.0 ± 1.7	7.9 ± 1.1	8.7 ± 1.9
Eroded surface/bone surface (%)	8.3 ± 5.8	6.1 ± 2.3	6.2 ± 2.4	7.5 ± 2.2
Dynamic histomorphometry				
Mineral apposition rate (μm/day)	2.3 ± 0.3	4.0 ± 0.8[a]	2.9 ± 0.9	3.9 ± 1.2
Mineralizing surface/bone surface (%)	2.9 ± 0.7	3.8 ± 2.5	4.1 ± 2.0	6.0 ± 3.5
Bone formation rate (μm^3/μm^2/day)	0.07 ± 0.02	0.15 ± 0.09	0.12 ± 0.06	0.21 ± 0.09

[a] Significantly different between control and *Notch3*$^{tm1.1Ecan}$, $p < 0.05$ by unpaired *t* test.
[b] $p < 0.055$.

Table 4

Cancellous bone histomorphometry of 4-month-old *Notch3*$^{tm1.1Ecan}$ male and female mutant mice and control littermates

Bone histomorphometry was performed on sagittal sections of distal femora from 4-month-old male and female *Notch3*$^{tm1.1Ecan}$ mutant mice and sex-matched control littermates. Values are means ± S.D.

	Males		Females	
Distal femur trabecular bone	Control ($n = 8$)	*Notch3*$^{tm1.1Ecan}$ ($n = 7$)	Control ($n = 5$)	*Notch3*$^{tm1.1Ecan}$ ($n = 6$)
Bone volume/tissue volume (%)	11.0 ± 2.4	8.0 ± 2.0[a]	5.7 ± 3.3	7.4 ± 2.4
Trabecular separation (μm)	326 ± 52	455 ± 93[a]	718 ± 257	481 ± 160
Trabecular number (1/mm)	2.8 ± 0.4	2.1 ± 0.4[a]	1.5 ± 0.6	2.1 ± 0.6
Trabecular thickness (μm)	40.3 ± 11.5	38.5 ± 8.1	38.0 ± 6.4	36.0 ± 4.6
Osteoblast surface/bone surface (%)	7.7 ± 2.6	12.7 ± 3.3[a]	9.2 ± 0.8	10.3 ± 2.2
Osteoblasts/bone perimeter (1/mm)	6.8 ± 1.9	10.8 ± 3.4[a]	7.7 ± 1.5	7.8 ± 3.8
Osteoid surface/bone surface (%)	0.7 ± 0.4	1.5 ± 0.6[a]	1.0 ± 1.0	1.2 ± 0.8
Osteocytes/bone area (mm^2)	599 ± 118	660 ± 99	735 ± 205	779 ± 148
Osteoclast surface/bone surface (%)	8.1 ± 2.5	10.2 ± 2.9	13.5 ± 7.5	14.9 ± 6.0
Osteoclasts/bone perimeter (1/mm)	3.2 ± 0.9	4.1 ± 1.2	5.4 ± 2.5	5.5 ± 2.2
Eroded surface/bone surface (%)	3.3 ± 1.0	3.7 ± 1.0	4.7 ± 3.5	5.1 ± 1.7
Mineral apposition rate (μm/day)	0.8 ± 0.2	1.0 ± 0.1	1.2 ± 0.1	1.6 ± 0.3
Mineralizing surface/bone surface (%)	6.5 ± 1.1	9.8 ± 4.7	8.9 ± 1.6	10.0 ± 5.0
Bone formation rate (μm^3/μm^2/day)	0.05 ± 0.02	0.09 ± 0.04[a]	0.11 ± 0.02	0.15 ± 0.09

[a] Significantly different between control and *Notch3*$^{tm1.1Ecan}$, $p < 0.05$ by unpaired *t* test.

uration and causes marked osteopenia, whereas NOTCH2 gain of function causes osteopenia secondary to an increase in osteoclast number and bone resorption (22, 26, 50). In contrast to the inhibitory actions of Notch1 and Notch2 on osteoblastogenesis, Notch3 gain of function enhanced osteoblast replication and function, establishing a distinct role of Notch3 in the skeleton. Although Notch2 and Notch3 enhance osteoclastogenesis, the mechanisms appear to be distinct. Notch2 is expressed by osteoclasts and has direct as well as osteoblast-dependent effects on osteoclastogenesis, whereas Notch3 is not expressed in cells of the myeloid/osteoclast lineage and enhances osteoclast differentiation by inducing RANKL and suppressing osteoprotegerin in the osteoblast lineage (20, 26). Notch3, like Notch1 and Notch2, induced the expression of Notch canonical target genes. It is reasonable to believe that the Notch3 NICD and RBPJκ have interactions distinct from the interactions of the Notch1 or Notch2 NICD; this would result in specific downstream events not shared by either Notch1 or Notch2 (19). Another source of the different actions of Notch receptors relates to their pattern of cellular expression as shown in the present work.

Although the goal was to replicate LMS, a limitation of the work is the use of a global mutation, so systemic or indirect consequences of the mutant *Notch3*$^{tm1.1Ecan}$ in bone cannot be excluded. However, no obvious neurological alterations were observed in mutant mice, and histopathology of multiple organs revealed no abnormalities. Other limitations of the work relate to the use of the CRISPR/Cas9 approach to create the *Notch3*$^{tm1.1Ecan}$ mouse model because it could have resulted in off-target effects. However, most of the off-target effects reported with CRISPR/Cas9 technology have used human-induced pluripotent or embryonic stem cells transfected with Cas9 and sgRNA expression vectors, generating Cas9 and sgRNA in significant amounts for a prolonged period of time and therefore increasing the possibility of off-target effects (51, 52). A limited amount of *Cas9* mRNA and sgRNA was injected into one-cell embryos to create the *Notch3*$^{tm1.1Ecan}$ mutants described, decreasing the likelihood of off-target effects. Moreover, the sgRNA selected scored high by inverse likelihood of off-target binding, and we did not detect a change in phenotype following three to four rounds of matings of *Notch3*$^{tm1.1Ecan}$ heterozygous mice with WT mice (53). This suggests that off-

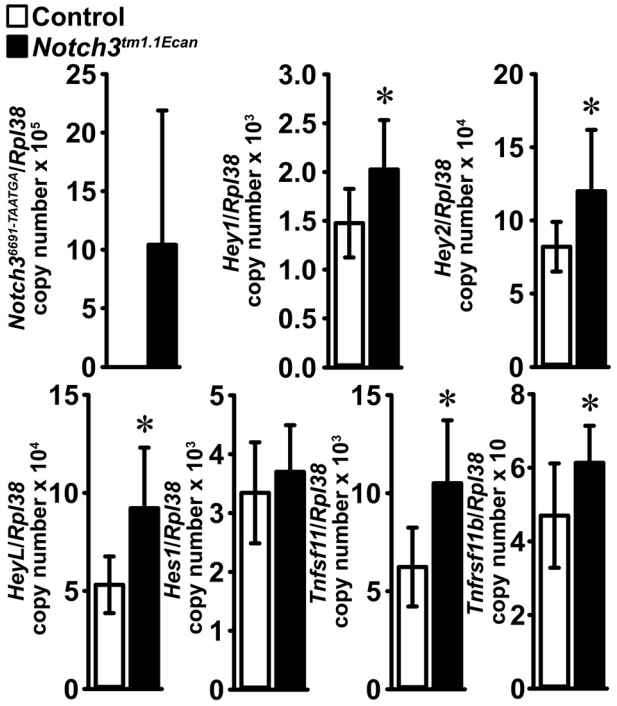

Figure 4. *Notch3*$^{6691\text{-}TAATGA}$, *Hey1*, *Hey2*, *HeyL*, *Hes1*, *Tnfsf11* (RANKL), and *Tnfrsf11b* (osteoprotegerin) mRNA levels in tibiae from 1-month-old *Notch3*$^{tm1.1Ecan}$ mutant (*black bars*) and control littermate mice (*white bars*). Transcript levels are expressed as copy number corrected for *Rpl38*. Values are means ± S.D. (*error bars*); $n = 8$ for control; $n = 8$ for *Notch3*$^{tm1.1Ecan}$ for all transcripts with the exception of *Tnfsf11* where $n = 7$ for control. Data are derived from biological replicates. *, significantly different between *Notch3*$^{tm1.1Ecan}$ mutant and WT control, $p < 0.05$ by unpaired *t* test.

target effects, which should segregate out, are not responsible for the phenotype.

Notch3 is associated with a variety of pathological conditions in addition to LMS. Notch3 promotes tumor cell proliferation and has been implicated in the bone-invasive potential of carcinoma of the breast and multiple myeloma and in the pathogenesis of mandibular torus (27, 54–57). Mutations in the extracellular domain of *NOTCH3* cause cerebral autosomal-dominant arteriopathy with subcortical infarcts and leukoencephalopathy syndrome (CADASIL) (58–60). This cerebral vascular disorder is characterized by strokes at a young age and accumulation of NOTCH3 in small vessels of affected individuals (61).

In conclusion, *Notch3*$^{tm1.1Ecan}$ mice harboring a mutation analogous to that found in subjects with LMS exhibit marked osteopenia despite an increase in osteoblast proliferation and function. The osteopenia is associated with enhanced RANKL and suppressed osteoprotegerin expression by cells of the osteoblast lineage.

Experimental procedures

Lateral meningocele mutant mice (Notch3$^{tm1.1Ecan}$*)*

RNA-guided CRISPR-associated Cas9 nuclease technology was used to create a mutation mimicking that found in a subject afflicted by LMS at the Center for Mouse Genome Modification of UConn Health (31–34). The subject harbored a single bp insertion at c.6692_93insC (from the start of translation) of *NOTCH3*, predicting the premature termination of a protein product devoid of the PEST domain. To engineer the *Notch3*$^{tm1.1Ecan}$ global mutant allele, the corresponding human *NOTCH3* mutation was introduced into the mouse genome (6691–6696 ACCAAG→TAATGA), leading to a T2231X change at the amino acid level and creating a truncated protein of 2230 amino acids (*versus* 2318 in wildtype) devoid of the PEST domain. The databases http://zifit.partners.org/ZiFiT/[5] (80, 81) and http://crispr.mit.edu[5] were utilized to evaluate potential sgRNAs, and *Notch3* sgRNA 5′-AACCCGCAGUAG-CCCCACCA was selected because of its high score and limited probabilities of off-target effects and designed to cleave between nucleotides 6691 and 6692 of exon 33 of *Notch3* adjacent to a protospacer adjacent motif (Fig. 1). A synthetic DNA fragment containing a T7 promoter driving sequences coding for *Notch3* sgRNA was used as a template to synthesize the sgRNA. A single-strand DNA of 146 nucleotides containing the tandem stop codon TAATGA and 70 nucleotides of *Notch3* homologous 5′- and 3′-arms (Fig. 1) were coinjected into C57BL/6J one-cell embryos with *Notch3* sgRNA and *Cas9* mRNA. Injected embryos were transferred into CD1 pseudopregnant foster females, and progeny were screened by PCR. The proper insertion of the *Notch3* 6691–6696 ACCAAG→TAATGA mutation was confirmed by sequencing of genomic DNA obtained from ear punches from F1 mice (Fig. 1) (GENEWIZ, South Plainfield, NJ). Heterozygous F1 mice were crossed with C57BL/6J WT mice to establish the mutant mouse line. *Notch3*$^{tm1.1Ecan}$ heterozygous mutant mice were crossed with WT mice to generate *Notch3*$^{tm1.1Ecan}$ mutants and sex-matched littermate controls in a C57BL/6J genetic background for study. Genotypes were determined by PCR analysis of tail DNA using forward primer 5′-GTGCTCAGCTTTGGTCTG-CTC-3′ and reverse primer 5′-CGCAGGAAGCGCGCTCA-TTA-3′ for *Notch3*$^{tm1.1Ecan}$ or 5′-CGCAGGAAGCGGGCCT-TGG-3′ for the WT allele (Integrated DNA Technologies, Coralville, IA). Studies were approved by the Institutional Animal Care and Use Committee of UConn Health.

Serum glucose and hormone assays

17β-Estradiol, murine PTH, and insulin were measured by ELISA assays in serum from *Notch3*$^{tm1.1Ecan}$ and control mice following an overnight fast using commercially available kits (17β-estradiol ELISA kit from Abcam, Cambridge, MA; murine insulin ELISA kit from Thermo Fisher Scientific, Waltham, MA; and mouse PTH(1–84) ELISA kit from Quidel Corp., San Diego, CA). Serum glucose was measured using an EnzyChrom glucose assay kit from BioAssay Systems (Hayward, CA).

Densitometry and body composition

Total body fat (grams) was measured on anesthetized mice using a PIXImus small animal DEXA system (GE Medical System/Lunar, Madison, WI) (62).

Microcomputed tomography

Femoral microarchitecture was determined using a μCT instrument (Scanco μCT 40, Scanco Medical AG, Bassersdorf,

[5] Please note that the JBC is not responsible for the long-term archiving and maintenance of this site or any other third party-hosted site.

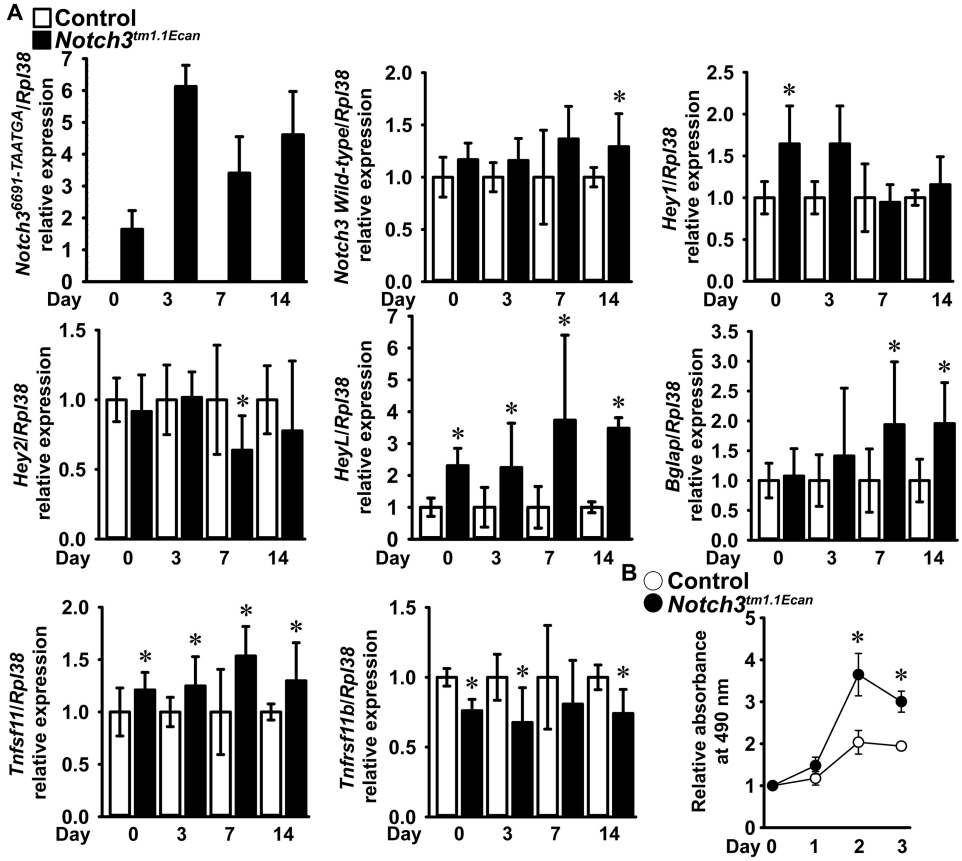

Figure 5. Cultured calvarial osteoblast-enriched cells from *Notch3*$^{tm1.1Ecan}$ mutant (*black bars; filled black circles*) and WT (*white bars; open circles*) littermate controls. *A*, total RNA was extracted, and gene expression was measured by qRT-PCR in the presence of specific primers and probes. Data are expressed as *Notch3*$^{6691\text{-}TAATGA}$ copy number corrected for *Rpl38* ($n = 4$) or relative expression of *Notch3*, *Hey1*, *Hey2*, *HeyL*, *Bglap*, *Tnfsf11* (RANKL), and *Tnfrsf11b* (osteoprotegerin) after correction for *Rpl38*. Values are means ± S.D. (*error bars*); number of observations for control, $n = 8$, and for *Notch3*$^{tm1.1Ecan}$, $n = 8$. Data were pooled from two experiments derived from technical replicates, and the control for each transcript (except *Notch3*$^{6691\text{-}TAATGA}$) was normalized to 1. *B*, change in the number of biochemically active cells estimated by measuring absorbance at 490 nm following a 4-h exposure to MTT. Data from control or *Notch3*$^{tm1.1Ecan}$ cells at day 0 are normalized to 1. Values are means ± S.D. (*error bars*); number of observations for control, $n = 4$, and for *Notch3*$^{tm1.1Ecan}$, $n = 4$ with the exception of *Notch3*$^{tm1.1Ecan}$ at day 1 where $n = 3$. Data are derived from technical replicates. *, significantly different between *Notch3*$^{tm1.1Ecan}$ mutant and WT control cells, $p < 0.05$ in *A* by unpaired *t* test and in *B* by ANOVA with Holm–Šídák post hoc analysis.

Switzerland), which was calibrated periodically using a phantom provided by the manufacturer (63, 64). Femora were scanned in 70% ethanol at high resolution, energy level of 55 peak kilovoltage (kVp), intensity of 145 μA, and integration time of 200 ms as reported previously (26, 50). A total of 100 slices at midshaft and 160 slices at the distal metaphysis were acquired at an isotropic voxel size of 216 μm^3 and a slice thickness of 6 μm and chosen for analysis. Cancellous bone volume fraction (bone volume/total volume) and microarchitecture were evaluated starting ~1.0 mm proximal from the femoral condyles. Contours were manually drawn every 10 slices, a few voxels away from the endocortical boundary, to define the region of interest for analysis, whereas the remaining slice contours were iterated automatically. Total volume, bone volume, bone volume fraction, trabecular thickness, trabecular number, connectivity density, structure model index, and material density were measured in trabecular regions using a Gaussian filter ($\sigma = 0.8$) and user-defined thresholds (63, 64). For analysis of cortical bone, contours were iterated across 100 slices along the cortical shell of the femoral midshaft, excluding the marrow cavity. Analysis of bone volume/total volume, porosity, cortical thickness, total cross-sectional and cortical bone area, periosteal and endosteal perimeter, and material density were conducted using a Gaussian filter ($\sigma = 0.8$, support = 1) with operator-defined thresholds.

Bone histomorphometry

Bone histomorphometry was carried out in 1- and 4-month-old mice injected with 20 mg/kg calcein and 50 mg/kg demeclocycline at a 2- and 7-day interval, respectively, and sacrificed 2 days after demeclocycline administration as reported previously (26, 50). Femora were dissected, fixed in 70% ethanol, and embedded in methyl methacrylate. For cancellous bone analysis, bones were sectioned at a thickness of 5 μm along the sagittal plane on a Microm microtome (Richards-Allan Scientific, Kalamazoo, MI) and stained with 0.1% toluidine blue. Static and dynamic parameters of bone morphometry were measured in a defined area between 0.35 and 2.16 mm from the growth plate at a magnification of 100× using an OsteoMeasure morphometry system (Osteometrics, Atlanta, GA). Stained sections were used to measure trabecular bone area; trabecular number and thickness; osteoblast, osteocyte, and osteoclast number; and osteoid and eroded surface. Mineralizing surface per bone surface and mineral apposition rate were measured on unstained

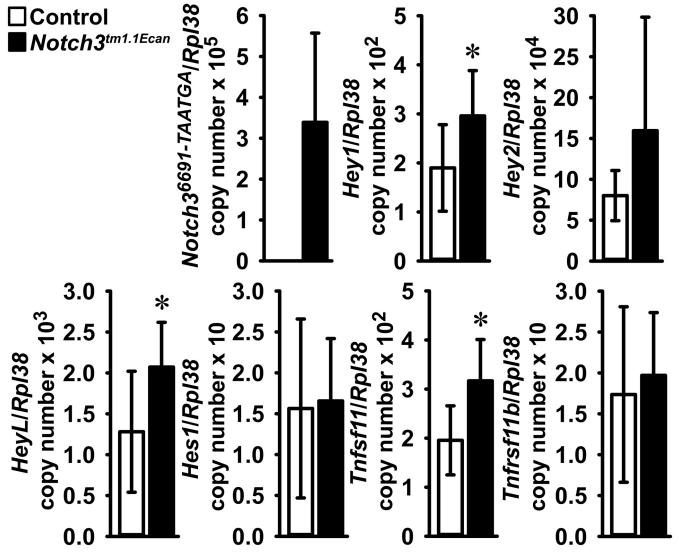

Figure 6. Isolated osteocyte-enriched cells from *Notch3*$^{tm1.1Ecan}$ mutant (*black bars*) and WT (*white bars*) littermate controls. Total RNA was extracted, and gene expression was measured by qRT-PCR in the presence of specific primers and probes. Data are expressed as *Notch3*$^{6691\text{-}TAATGA}$, *Hey1*, *Hey2*, *HeyL*, *Hes1*, *Tnfsf11* (RANKL), and *Tnfrsf11b* (osteoprotegerin) copy number corrected for *Rpl38*. Values are means ± S.D. (*error bars*); number of observations for control, $n = 7$, and for *Notch3*$^{tm1.1Ecan}$, $n = 7$. Date are derived from biological replicates. *, significantly different between *Notch3*$^{tm1.1Ecan}$ mutant and WT control cells, $p < 0.05$ by unpaired *t* test.

sections visualized under UV light and a triple diamidino-2-phenylindole/fluorescein/Texas Red set long-pass filter, and bone formation rate was calculated. Terminology and units used for cancellous and cortical bone histomorphometry are those recommended by the Histomorphometry Nomenclature Committee of the American Society for Bone and Mineral Research (65, 66).

Osteoblast-enriched cell cultures and cell viability assay

Parietal bones from 3–5-day-old *Notch3*$^{tm1.1Ecan}$ mice and littermate controls were exposed to 1.2 units/ml Liberase TL (Sigma-Aldrich) for 20 min at 37 °C, and cells were extracted in five consecutive reactions (67). Cells from the last three digestions were pooled and seeded at a density of 10,000 cells/cm^2 as described previously (50, 68). Osteoblast-enriched cells were cultured in Dulbecco's modified Eagle's medium supplemented with nonessential amino acids (both from Thermo Fisher Scientific), 20 mM HEPES, 100 μg/ml ascorbic acid (both from Sigma-Aldrich), and 10% heat-inactivated fetal bovine serum (FBS; Atlanta Biologicals, Norcross, GA) in a humidified 5% CO_2 incubator at 37 °C. The number of biochemically active osteoblasts was estimated by measuring the product of MTT reduction to formazan with the Vybrant MTT cell proliferation assay kit (Thermo Fisher Scientific) according to the manufacturer's instructions (69).

Osteocyte-enriched cultures

Osteocyte-enriched cells were obtained following a modification of a method described previously (26, 35). Femora were removed aseptically from 1-month-old experimental and control mice. The surrounding tissues was dissected, the proximal epiphyseal end was excised, and the bone marrow was removed by centrifugation. The distal epiphysis was excised, and femora were digested for 20 min at 37 °C with type II bacterial collagenase pretreated with *N*-α-tosyl-L-lysyl-chloromethyl ketone hydrochloride and subsequently exposed to 5 mM EDTA for 10 min at 37 °C. The resulting osteocyte-enriched cortical femora were cultured individually in Dulbecco's modified Eagle's medium supplemented with nonessential amino acids (both from Life Technologies), 100 μg/ml ascorbic acid, and 10% FBS for 3 days at 37 °C in a humidified 5% CO_2 incubator as described (26).

Culture of BMMs and osteoclast formation

To obtain BMMs, the marrow from *Notch3*$^{tm1.1Ecn}$ mice and littermate controls was removed by flushing with a 26-gauge needle, and erythrocytes were lysed in 150 mM NH_4Cl, 10 mM $KHCO_3$, and 0.1 mM EDTA (pH 7.4) as described previously (26, 50, 70). Cells were centrifuged, and the sediment was suspended in α-minimum essential medium (α-MEM) (Thermo Fisher Scientific) in the presence of 10% FBS and recombinant human M-CSF at 30 ng/ml as described (50). M-CSF cDNA and expression vector were obtained from D. Fremont (Washington University, St. Louis, MO), and M-CSF was purified as reported previously (71). Cells were seeded on uncoated plastic Petri dishes at a density of 300,000 cells/cm^2 and cultured for 3–4 days. For osteoclast formation, cells were collected following treatment with 0.25% trypsin and EDTA for 5 min and seeded on tissue culture plates at a density of 47,000 cells/cm^2 in α-MEM with 10% FBS, 30 ng/ml M-CSF, and 10 ng/ml recombinant murine RANKL. *Tnfsf11* cDNA, encoding RANKL, and expression vector were obtained from M. Glogauer (Toronto, Canada), and glutathione *S*-transferase–tagged RANKL was expressed and purified as described (72). To determine the contribution of osteoblast-derived factors to osteoclast formation, calvarial osteoblast-enriched cells from *Notch3*$^{tm1.1Ecan}$ mutant and WT control littermates were seeded at a density of 15,700 cells/cm^2 in α-MEM in the presence of BMMs from either genotype at a density of 47,000 cells/cm^2 and cultured with 1,25-dihydroxyvitamin D_3 at 10 nM. Cultures were carried out until the formation of multinucleated TRAP-positive cells was achieved. TRAP enzyme histochemistry was conducted using a commercial kit (Sigma-Aldrich), in accordance with the manufacturer's instructions, as reported previously (50). TRAP-positive cells containing three or more nuclei were considered osteoclasts.

Quantitative reverse transcription–polymerase chain reaction

Total RNA was extracted from cells with the RNeasy kit (Qiagen, Valencia, CA) and from homogenized tibiae or osteocyte-enriched femoral fragments, following the removal of the bone marrow by centrifugation, with the micro RNeasy kit (Qiagen), in accordance with the manufacturer's instructions, as reported previously (26, 50, 73, 74). The integrity of the RNA from tibiae and osteocyte-rich fragments was assessed by microfluidic electrophoresis on an Experion instrument (Bio-Rad), and only RNA with a quality indicator number equal to or higher than 7.0 was used for subsequent analysis. Equal amounts of RNA were reverse transcribed using the iScript RT-PCR kit (Bio-Rad) and amplified in the presence of specific primers (Inte-

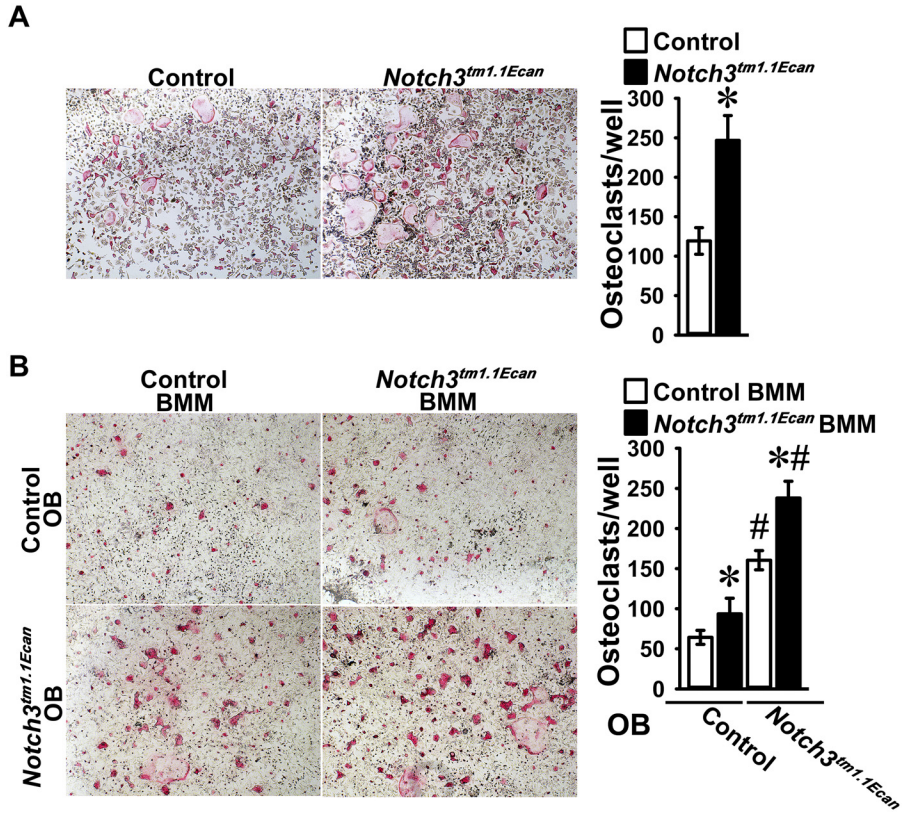

Figure 7. BMMs harvested from long bones of *Notch3*$^{tm1.1Ecan}$ mutants (*black bars*) and WT littermate controls (*white bars*) cultured for 72 h in the presence of M-CSF at 30 ng/ml. In *A*, cells were seeded on culture dishes in the presence of M-CSF at 30 ng/ml and RANKL at 10 ng/ml and assessed for the appearance of osteoclasts defined as TRAP-positive multinucleated cells. In *B*, BMMs from control and *Notch3*$^{tm1.1Ecan}$ mutant mice were seeded on culture dishes in the presence of osteoblasts (*OB*) from control or *Notch3*$^{tm1.1Ecan}$ mutant mice with 1,25-dihydroxyvitamin D_3 at 10 nM and assessed for the appearance of TRAP-positive multinucleated cells. Representative images of TRAP-stained multinucleated cells are shown in the *left panels*. Data are expressed as total number of TRAP-positive multinucleated cells/well. Values are means ± S.D. (*error bars*); $n = 4$ technical replicates. *, significantly different between *Notch3*$^{tm1.1Ecan}$ and WT control BMMs, $p < 0.05$ in *A* by unpaired *t* test and in *B* by ANOVA with Holm–Šídák post hoc analysis. #, significantly different between *Notch3*$^{tm1.1Ecan}$ and WT osteoblasts by ANOVA.

Table 5

Primers used for qRT-PCR determinations

GenBank accession numbers identify transcript recognized by primer pairs.

Gene	Strand	Sequence (5′–3′)	GenBank accession no.
Bglap	Forward	5′-GACTCCGGCGCTACCTTGGGTAAG-3′	NM_001037939
	Reverse	5′-CCCAGCACAACTCCTCCCTA-3′	
Hes1	Forward	5′-ACCAAAGACGGCCTCTGAGCACAGAAAGT-3′	NM_008235
	Reverse	5′-ATTCTTGCCCTTCGCCTCTT-3′	
Hey1	Forward	5′-ATCTCAACAACTACGCATCCCAGC-3′	NM_010423
	Reverse	5′-GTGTGGGTGATGTCCGAAGG-3′	
Hey2	Forward	5′-AGCGAGAACAATTACCCTGGGCAC-3′	NM_013904
	Reverse	5′-GGTAGTTGTCGGTGAATTGGACCT-3′	
HeyL	Forward	5′-CAGTAGCCTTTCTGAATTGCGAC-3′	NM_013905
	Reverse	5′-AGCTTGGAGGAGCCCTGTTTC-3′	
Notch3	Forward	5′-CCGATTCTCCTGTCGTTGTCTCC-3′	NM_008716
	Reverse	5′-TGAACACAGGGCCTGCTGAC-3′	
Notch3$^{6691\text{-}TAATGA}$	Forward	5′-AACCCGCAGTAGCCCCTAATG-3′	Not applicable
	Reverse	5′-ATAAGGATGCTCGCTGGGAACC-3′	
Rpl38	Forward	5′-AGAACAAGGATAATGTGAAGTTCAAGGTTC-3′	NM_001048057; NM_001048058; NM_023372
	Reverse	5′-CTGCTTCAGCTTCTCTGCCTTT-3′	
Tnfrsf11b	Forward	5′-CAGAAAGGAAATGCAACACATGACAAC-3′	NM_008764
	Reverse	5′-GCCTCTTCACACAGGGTGACATC-3′	
Tnfsf11	Forward	5′-TATAGAATCCTGAGACTCCATGAAAAC-3′	NM_011613
	Reverse	5′-CCCTGAAAGGCTTGTTTCATCC-3′	

grated DNA Technologies) (Table 5) with iQ SYBR Green Supermix or SsoAdvanced Universal SYBR Green Supermix (Bio-Rad) at 60 °C for 35 cycles. Transcript copy number was estimated by comparison with a serial dilution of cDNA for *Bglap* (encoding for osteocalcin; from J. Lian, University of Vermont, Burlington, VT), *Hey1* and *Hey2* (both from T. Iso,

Gunma University, Gunma, Japan), *HeyL* (from D. Srivastava, Gladstone Institute of Cardiovascular Disease, San Francisco, CA), *Tnfsf11* (from Source BioScience, Nottingham, UK), or *Tnfrsf11b* (from American Type Tissue Culture Collection (ATCC), Manassas, VA) (75–77). *Notch3*$^{tm1.1Ecan}$ transcript copy number was estimated by comparison with a serial dilution of a synthetic DNA fragment (Integrated DNA Technologies) containing ~90 bp surrounding the *Notch3* 6691–6696 ACCAAG→TAATGA mutation and cloned into pcDNA3.1(−) (Life Technologies) by isothermal single-reaction assembly using commercially available reagents (New England Biolabs, Ipswich, MA) (78). Amplification reactions were conducted in a CFX96 qRT-PCR detection system (Bio-Rad), and fluorescence was monitored during every PCR cycle at the annealing step. Data are expressed as copy number or relative transcript expression, both corrected for *Rpl38* (from ATCC) (79).

Statistics

Data are expressed as means ± S.D. All data except for osteoblast and BMM cultures represent biological replicates. qRT-PCR values were derived from two technical replicates of biological replicates as indicated in the text and tables. Statistical differences were determined by unpaired Student's *t* test or analysis of variance (ANOVA) with Holm–Šídák post hoc analysis for pairwise or multiple comparisons.

Author contributions—E. C. conceptualization; E. C., J. Y., and S. Z. formal analysis; E. C. funding acquisition; E. C. investigation; E. C. writing-original draft; E. C., J. Y., L. S., and S. Z. writing-review and editing; J. Y., L. S., S.-P. Y., and S. Z. methodology.

Acknowledgments—We thank J. Lian for Bglap cDNA, T. Iso for Hey1 and Hey2 cDNAs, D. Srivastava for HeyL cDNA, D. Bridgewater and T. Eller for technical assistance, and M. Yurczak for secretarial support.

References

1. Zanotti, S., and Canalis, E. (2016) Notch signaling and the skeleton. *Endocr. Rev.* **37,** 223–253 CrossRef Medline
2. Artavanis-Tsakonas, S., Rand, M. D., and Lake, R. J. (1999) Notch signaling: cell fate control and signal integration in development. *Science* **284,** 770–776 CrossRef Medline
3. Lindsell, C. E., Boulter, J., diSibio, G., Gossler, A., and Weinmaster, G. (1996) Expression patterns of Jagged, Delta1, Notch1, Notch2, and Notch3 genes identify ligand-receptor pairs that may function in neural development. *Mol. Cell. Neurosci.* **8,** 14–27 CrossRef Medline
4. Cordle, J., Redfieldz, C., Stacey, M., van der Merwe, P. A., Willis, A. C., Champion, B. R., Hambleton, S., and Handford, P. A. (2008) Localization of the Delta-like-1-binding site in human Notch-1 and its modulation by calcium affinity. *J. Biol. Chem.* **283,** 11785–11793 CrossRef Medline
5. Sanchez-Irizarry, C., Carpenter, A. C., Weng, A. P., Pear, W. S., Aster, J. C., and Blacklow, S. C. (2004) Notch subunit heterodimerization and prevention of ligand-independent proteolytic activation depend, respectively, on a novel domain and the LNR repeats. *Mol. Cell. Biol.* **24,** 9265–9273 CrossRef Medline
6. Kovall, R. A. (2008) More complicated than it looks: assembly of Notch pathway transcription complexes. *Oncogene* **27,** 5099–5109 CrossRef Medline
7. Kovall, R. A. (2007) Structures of CSL, Notch and Mastermind proteins: piecing together an active transcription complex. *Curr. Opin. Struct. Biol.* **17,** 117–127 CrossRef Medline
8. Ohtsuka, T., Ishibashi, M., Gradwohl, G., Nakanishi, S., Guillemot, F., and Kageyama, R. (1999) Hes1 and Hes5 as notch effectors in mammalian neuronal differentiation. *EMBO J.* **18,** 2196–2207 CrossRef Medline
9. Iso, T., Sartorelli, V., Poizat, C., Iezzi, S., Wu, H. Y., Chung, G., Kedes, L., and Hamamori, Y. (2001) HERP, a novel heterodimer partner of HES/E(spl) in Notch signaling. *Mol. Cell. Biol.* **21,** 6080–6089 CrossRef Medline
10. Iso, T., Kedes, L., and Hamamori, Y. (2003) HES and HERP families: multiple effectors of the Notch signaling pathway. *J. Cell. Physiol.* **194,** 237–255 CrossRef Medline
11. Kopan, R., and Ilagan, M. X. (2009) The canonical Notch signaling pathway: unfolding the activation mechanism. *Cell* **137,** 216–233 CrossRef Medline
12. Zanotti, S., and Canalis, E. (2010) Notch and the skeleton. *Mol. Cell. Biol.* **30,** 886–896 CrossRef Medline
13. Bai, S., Kopan, R., Zou, W., Hilton, M. J., Ong, C. T., Long, F., Ross, F. P., and Teitelbaum, S. L. (2008) NOTCH1 regulates osteoclastogenesis directly in osteoclast precursors and indirectly via osteoblast lineage cells. *J. Biol. Chem.* **283,** 6509–6518 CrossRef Medline
14. Zanotti, S., and Canalis, E. (2017) Parathyroid hormone inhibits Notch signaling in osteoblasts and osteocytes. *Bone* **103,** 159–167 CrossRef Medline
15. Swiatek, P. J., Lindsell, C. E., del Amo, F. F., Weinmaster, G., and Gridley, T. (1994) Notch1 is essential for postimplantation development in mice. *Genes Dev.* **8,** 707–719 CrossRef Medline
16. Weinmaster, G., Roberts, V. J., and Lemke, G. (1992) Notch2: a second mammalian Notch gene. *Development* **116,** 931–941 Medline
17. McCright, B., Gao, X., Shen, L., Lozier, J., Lan, Y., Maguire, M., Herzlinger, D., Weinmaster, G., Jiang, R., and Gridley, T. (2001) Defects in development of the kidney, heart and eye vasculature in mice homozygous for a hypomorphic Notch2 mutation. *Development* **128,** 491–502 Medline
18. Wu, J., and Bresnick, E. H. (2007) Bare rudiments of notch signaling: how receptor levels are regulated. *Trends Biochem. Sci.* **32,** 477–485 CrossRef Medline
19. Yuan, Z., Friedmann, D. R., VanderWielen, B. D., Collins, K. J., and Kovall, R. A. (2012) Characterization of CSL (CBF-1, Su(H), Lag-1) mutants reveals differences in signaling mediated by Notch1 and Notch2. *J. Biol. Chem.* **287,** 34904–34916 CrossRef Medline
20. Fukushima, H., Nakao, A., Okamoto, F., Shin, M., Kajiya, H., Sakano, S., Bigas, A., Jimi, E., and Okabe, K. (2008) The association of Notch2 and NF-κB accelerates RANKL-induced osteoclastogenesis. *Mol. Cell. Biol.* **28,** 6402–6412 CrossRef Medline
21. Canalis, E., Adams, D. J., Boskey, A., Parker, K., Kranz, L., and Zanotti, S. (2013) Notch signaling in osteocytes differentially regulates cancellous and cortical bone remodeling. *J. Biol. Chem.* **288,** 25614–25625 CrossRef Medline
22. Canalis, E., Parker, K., Feng, J. Q., and Zanotti, S. (2013) Osteoblast lineage-specific effects of Notch activation in the skeleton. *Endocrinology* **154,** 623–634 CrossRef Medline
23. Engin, F., Yao, Z., Yang, T., Zhou, G., Bertin, T., Jiang, M. M., Chen, Y., Wang, L., Zheng, H., Sutton, R. E., Boyce, B. F., and Lee, B. (2008) Dimorphic effects of Notch signaling in bone homeostasis. *Nat. Med.* **14,** 299–305 CrossRef Medline
24. Hilton, M. J., Tu, X., Wu, X., Bai, S., Zhao, H., Kobayashi, T., Kronenberg, H. M., Teitelbaum, S. L., Ross, F. P., Kopan, R., and Long, F. (2008) Notch signaling maintains bone marrow mesenchymal progenitors by suppressing osteoblast differentiation. *Nat. Med.* **14,** 306–314 CrossRef Medline
25. Zanotti, S., Smerdel-Ramoya, A., Stadmeyer, L., Durant, D., Radtke, F., and Canalis, E. (2008) Notch inhibits osteoblast differentiation and causes osteopenia. *Endocrinology* **149,** 3890–3899 CrossRef Medline
26. Canalis, E., Schilling, L., Yee, S. P., Lee, S. K., and Zanotti, S. (2016) Hajdu Cheney mouse mutants exhibit osteopenia, increased osteoclastogenesis and bone resorption. *J. Biol. Chem.* **291,** 1538–1551 CrossRef Medline
27. Bellavia, D., Checquolo, S., Campese, A. F., Felli, M. P., Gulino, A., and Screpanti, I. (2008) Notch3: from subtle structural differences to functional diversity. *Oncogene* **27,** 5092–5098 CrossRef Medline

28. Lehman, R. A., Stears, J. C., Wesenberg, R. L., and Nusbaum, E. D. (1977) Familial osteosclerosis with abnormalities of the nervous system and meninges. *J. Pediatr.* **90,** 49–54 CrossRef Medline
29. Gripp, K. W., Scott, C. I., Jr., Hughes, H. E., Wallerstein, R., Nicholson, L., States, L., Bason, L. D., Kaplan, P., Zderic, S. A., Duhaime, A. C., Miller, F., Magnusson, M. R., and Zackai, E. H. (1997) Lateral meningocele syndrome: three new patients and review of the literature. *Am. J. Med. Genet.* **70,** 229–239 Medline
30. Avela, K., Valanne, L., Helenius, I., and Makitie, O. (2011) Hajdu-Cheney syndrome with severe dural ectasia. *Am. J. Med. Genet. A* **155A,** 595–598 CrossRefMedline
31. Gripp, K. W., Robbins, K. M., Sobreira, N. L., Witmer, P. D., Bird, L. M., Avela, K., Makitie, O., Alves, D., Hogue, J. S., Zackai, E. H., Doheny, K. F., Stabley, D. L., and Sol-Church, K. (2015) Truncating mutations in the last exon of NOTCH3 cause lateral meningocele syndrome. *Am. J. Med. Genet. A* **167A,** 271–281 CrossRefMedline
32. Wang, H., Yang, H., Shivalila, C. S., Dawlaty, M. M., Cheng, A. W., Zhang, F., and Jaenisch, R. (2013) One-step generation of mice carrying mutations in multiple genes by CRISPR/Cas-mediated genome engineering. *Cell* **153,** 910–918 CrossRef Medline
33. Yang, H., Wang, H., and Jaenisch, R. (2014) Generating genetically modified mice using CRISPR/Cas-mediated genome engineering. *Nat. Protoc.* **9,** 1956–1968 CrossRef Medline
34. Williams, A., Henao-Mejia, J., and Flavell, R. A. (2016) Editing the mouse genome using the CRISPR-Cas9 system. *Cold Spring Harb. Protoc.* **2016,** CrossRef Medline
35. Halleux, C., Kramer, I., Allard, C., and Kneissel, M. (2012) Isolation of mouse osteocytes using cell fractionation for gene expression analysis. *Methods Mol. Biol.* **816,** 55–66 CrossRef Medline
36. Nakamura, T., Imai, Y., Matsumoto, T., Sato, S., Takeuchi, K., Igarashi, K., Harada, Y., Azuma, Y., Krust, A., Yamamoto, Y., Nishina, H., Takeda, S., Takayanagi, H., Metzger, D., Kanno, J., *et al.* (2007) Estrogen prevents bone loss via estrogen receptor alpha and induction of Fas ligand in osteoclasts. *Cell* **130,** 811–823 CrossRef Medline
37. Novack, D. V. (2007) Estrogen and bone: osteoclasts take center stage. *Cell Metab.* **6,** 254–256 CrossRef Medline
38. Manolagas, S. C. (2010) From estrogen-centric to aging and oxidative stress: a revised perspective of the pathogenesis of osteoporosis. *Endocr. Rev.* **31,** 266–300 CrossRef Medline
39. Rogers, S., Wells, R., and Rechsteiner, M. (1986) Amino acid sequences common to rapidly degraded proteins: the PEST hypothesis. *Science* **234,** 364–368 CrossRef Medline
40. Rossi, D., Trifonov, V., Fangazio, M., Bruscaggin, A., Rasi, S., Spina, V., Monti, S., Vaisitti, T., Arruga, F., Famà, R., Ciardullo, C., Greco, M., Cresta, S., Piranda, D., Holmes, A., *et al.* (2012) The coding genome of splenic marginal zone lymphoma: activation of NOTCH2 and other pathways regulating marginal zone development. *J. Exp. Med.* **209,** 1537–1551 CrossRef Medline
41. Weng, A. P., Ferrando, A. A., Lee, W., Morris J. P., 4th, Silverman, L. B., Sanchez-Irizarry, C., Blacklow, S. C., Look, A. T., and Aster, J. C. (2004) Activating mutations of NOTCH1 in human T cell acute lymphoblastic leukemia. *Science* **306,** 269–271 CrossRef Medline
42. Breit, S., Stanulla, M., Flohr, T., Schrappe, M., Ludwig, W. D., Tolle, G., Happich, M., Muckenthaler, M. U., and Kulozik, A. E. (2006) Activating NOTCH1 mutations predict favorable early treatment response and long-term outcome in childhood precursor T-cell lymphoblastic leukemia. *Blood* **108,** 1151–1157 CrossRef Medline
43. Gripp, K. W. (2011) Lateral meningocele syndrome and Hajdu-Cheney syndrome: different disorders with overlapping phenotypes. *Am. J. Med. Genet. A* **155A**, 1773–1774 CrossRefMedline
44. Isidor, B., Lindenbaum, P., Pichon, O., Bézieau, S., Dina, C., Jacquemont, S., Martin-Coignard, D., Thauvin-Robinet, C., Le Merrer, M., Mandel, J. L., David, A., Faivre, L., Cormier-Daire, V., Redon, R., and Le Caignec, C. (2011) Truncating mutations in the last exon of NOTCH2 cause a rare skeletal disorder with osteoporosis. *Nat. Genet.* **43,** 306–308 CrossRef Medline
45. Simpson, M. A., Irving, M. D., Asilmaz, E., Gray, M. J., Dafou, D., Elmslie, F. V., Mansour, S., Holder, S. E., Brain, C. E., Burton, B. K., Kim, K. H., Pauli, R. M., Aftimos, S., Stewart, H., Kim, C. A., *et al.* (2011) Mutations in NOTCH2 cause Hajdu-Cheney syndrome, a disorder of severe and progressive bone loss. *Nat. Genet.* **43,** 303–305 CrossRef Medline
46. Aguirre, J. I., Plotkin, L. I., Stewart, S. A., Weinstein, R. S., Parfitt, A. M., Manolagas, S. C., and Bellido, T. (2006) Osteocyte apoptosis is induced by weightlessness in mice and precedes osteoclast recruitment and bone loss. *J. Bone Miner. Res.* **21,** 605–615 CrossRef Medline
47. Nakashima, T., Hayashi, M., Fukunaga, T., Kurata, K., Oh-Hora, M., Feng, J. Q., Bonewald, L. F., Kodama, T., Wutz, A., Wagner, E. F., Penninger, J. M., and Takayanagi, H. (2011) Evidence for osteocyte regulation of bone homeostasis through RANKL expression. *Nat. Med.* **17,** 1231–1234 CrossRef Medline
48. Plotkin, L. I., Gortazar, A. R., Davis, H. M., Condon, K. W., Gabilondo, H., Maycas, M., Allen, M. R., and Bellido, T. (2015) Inhibition of osteocyte apoptosis prevents the increase in osteocytic receptor activator of nuclear factor κB ligand (RANKL) but does not stop bone resorption or the loss of bone induced by unloading. *J. Biol. Chem.* **290,** 18934–18942 CrossRef Medline
49. Xiong, J., Onal, M., Jilka, R. L., Weinstein, R. S., Manolagas, S. C., and O'Brien, C. A. (2011) Matrix-embedded cells control osteoclast formation. *Nat. Med.* **17,** 1235–1241 CrossRef Medline
50. Zanotti, S., Yu, J., Sanjay, A., Schilling, L., Schoenherr, C., Economides, A. N., and Canalis, E. (2017) Sustained Notch2 signaling in osteoblasts, but not in osteoclasts, is linked to osteopenia in a mouse model of Hajdu-Cheney syndrome. *J. Biol. Chem.* **292,** 12232–12244 CrossRef Medline
51. Kim, D., Bae, S., Park, J., Kim, E., Kim, S., Yu, H. R., Hwang, J., Kim, J. I., and Kim, J. S. (2015) Digenome-seq: genome-wide profiling of CRISPR-Cas9 off-target effects in human cells. *Nat. Methods* **12,** 237–243 CrossRef Medline
52. Fu, Y., Foden, J. A., Khayter, C., Maeder, M. L., Reyon, D., Joung, J. K., and Sander, J. D. (2013) High-frequency off-target mutagenesis induced by CRISPR-Cas nucleases in human cells. *Nat. Biotechnol.* **31,** 822–826 CrossRef Medline
53. Iyer, V., Shen, B., Zhang, W., Hodgkins, A., Keane, T., Huang, X., and Skarnes, W. C. (2015) Off-target mutations are rare in Cas9-modified mice. *Nat. Methods* **12,** 479 CrossRef Medline
54. Konishi, J., Kawaguchi, K. S., Vo, H., Haruki, N., Gonzalez, A., Carbone, D. P., and Dang, T. P. (2007) γ-Secretase inhibitor prevents Notch3 activation and reduces proliferation in human lung cancers. *Cancer Res.* **67,** 8051–8057 CrossRef Medline
55. Zhang, Z., Wang, H., Ikeda, S., Fahey, F., Bielenberg, D., Smits, P., and Hauschka, P. V. (2010) Notch3 in human breast cancer cell lines regulates osteoblast-cancer cell interactions and osteolytic bone metastasis. *Am. J. Pathol.* **177,** 1459–1469 CrossRef Medline
56. Delgado-Calle, J., Anderson, J., Cregor, M. D., Hiasa, M., Chirgwin, J. M., Carlesso, N., Yoneda, T., Mohammad, K. S., Plotkin, L. I., Roodman, G. D., and Bellido, T. (2016) Bidirectional Notch signaling and osteocyte-derived factors in the bone marrow microenvironment promote tumor cell proliferation and bone destruction in multiple myeloma. *Cancer Res.* **76,** 1089–1100 CrossRef Medline
57. Dou, X. W., Park, W., Lee, S., Zhang, Q. Z., Carrasco, L. R., and Le, A. D. (2017) Loss of Notch3 signaling enhances osteogenesis of mesenchymal stem cells from mandibular torus. *J. Dent. Res.* **96,** 347–354 CrossRef Medline
58. Domenga, V., Fardoux, P., Lacombe, P., Monet, M., Maciazek, J., Krebs, L. T., Klonjkowski, B., Berrou, E., Mericskay, M., Li, Z., Tournier-Lasserve, E., Gridley, T., and Joutel, A. (2004) Notch3 is required for arterial identity and maturation of vascular smooth muscle cells. *Genes Dev.* **18,** 2730–2735 CrossRef Medline
59. Joutel, A. (2011) Pathogenesis of CADASIL: transgenic and knock-out mice to probe function and dysfunction of the mutated gene, Notch3, in the cerebrovasculature. *BioEssays* **33,** 73–80 CrossRef Medline
60. Joutel, A., Corpechot, C., Ducros, A., Vahedi, K., Chabriat, H., Mouton, P., Alamowitch, S., Domenga, V., Cécillion, M., Marechal, E., Maciazek, J., Vayssiere, C., Cruaud, C., Cabanis, E. A., Ruchoux, M. M., *et al.* (1996) Notch3 mutations in CADASIL, a hereditary adult-onset condition causing stroke and dementia. *Nature* **383,** 707–710 CrossRef Medline

61. Joutel, A., Andreux, F., Gaulis, S., Domenga, V., Cecillon, M., Battail, N., Piga, N., Chapon, F., Godfrain, C., and Tournier-Lasserve, E. (2000) The ectodomain of the Notch3 receptor accumulates within the cerebrovasculature of CADASIL patients. *J. Clin. Investig.* **105,** 597–605 CrossRef Medline
62. Nagy, T. R., Prince, C. W., and Li, J. (2001) Validation of peripheral dual-energy X-ray absorptiometry for the measurement of bone mineral in intact and excised long bones of rats. *J. Bone Miner. Res.* **16,** 1682–1687 CrossRef Medline
63. Bouxsein, M. L., Boyd, S. K., Christiansen, B. A., Guldberg, R. E., Jepsen, K. J., and Müller, R. (2010) Guidelines for assessment of bone microstructure in rodents using micro-computed tomography. *J. Bone Miner. Res.* **25,** 1468–1486 CrossRef Medline
64. Glatt, V., Canalis, E., Stadmeyer, L., and Bouxsein, M. L. (2007) Age-related changes in trabecular architecture differ in female and male C57BL/6J mice. *J. Bone Miner. Res.* **22,** 1197–1207 CrossRef Medline
65. Dempster, D. W., Compston, J. E., Drezner, M. K., Glorieux, F. H., Kanis, J. A., Malluche, H., Meunier, P. J., Ott, S. M., Recker, R. R., and Parfitt, A. M. (2013) Standardized nomenclature, symbols, and units for bone histomorphometry: a 2012 update of the report of the ASBMR Histomorphometry Nomenclature Committee. *J. Bone Miner. Res.* **28,** 2–17 CrossRef Medline
66. Parfitt, A. M., Drezner, M. K., Glorieux, F. H., Kanis, J. A., Malluche, H., Meunier, P. J., Ott, S. M., and Recker, R. R. (1987) Bone histomorphometry: standardization of nomenclature, symbols, and units. Report of the ASBMR Histomorphometry Nomenclature Committee. *J. Bone Miner. Res.* **2,** 595–610 Medline
67. Yesil, P., Michel, M., Chwalek, K., Pedack, S., Jany, C., Ludwig, B., Bornstein, S. R., and Lammert, E. (2009) A new collagenase blend increases the number of islets isolated from mouse pancreas. *Islets* **1,** 185–190 CrossRef Medline
68. Canalis, E., Zanotti, S., and Smerdel-Ramoya, A. (2014) Connective tissue growth factor is a target of Notch signaling in cells of the osteoblastic lineage. *Bone* **64,** 273–280 CrossRef Medline
69. Mosmann, T. (1983) Rapid colorimetric assay for cellular growth and survival: application to proliferation and cytotoxicity assays. *J. Immunol. Methods* **65,** 55–63 CrossRef Medline
70. Canalis, E., Sanjay, A., Yu, J., and Zanotti, S. (2017) An antibody to Notch2 reverses the osteopenic phenotype of Hajdu-Cheney mutant male mice. *Endocrinology* **158,** 730–742 CrossRef Medline
71. Lee, S. H., Rho, J., Jeong, D., Sul, J. Y., Kim, T., Kim, N., Kang, J. S., Miyamoto, T., Suda, T., Lee, S. K., Pignolo, R. J., Koczon-Jaremko, B., Lorenzo, J., and Choi, Y. (2006) v-ATPase V0 subunit d2-deficient mice exhibit impaired osteoclast fusion and increased bone formation. *Nat. Med.* **12,** 1403–1409 CrossRef Medline
72. Wang, Y., Lebowitz, D., Sun, C., Thang, H., Grynpas, M. D., and Glogauer, M. (2008) Identifying the relative contributions of Rac1 and Rac2 to osteoclastogenesis. *J. Bone Miner. Res.* **23,** 260–270 Medline
73. Nazarenko, I., Lowe, B., Darfler, M., Ikonomi, P., Schuster, D., and Rashtchian, A. (2002) Multiplex quantitative PCR using self-quenched primers labeled with a single fluorophore. *Nucleic Acids Res.* **30,** e37 CrossRef Medline
74. Nazarenko, I., Pires, R., Lowe, B., Obaidy, M., and Rashtchian, A. (2002) Effect of primary and secondary structure of oligodeoxyribonucleotides on the fluorescent properties of conjugated dyes. *Nucleic Acids Res.* **30,** 2089–2195 CrossRef Medline
75. Lian, J., Stewart, C., Puchacz, E., Mackowiak, S., Shalhoub, V., Collart, D., Zambetti, G., and Stein, G. (1989) Structure of the rat osteocalcin gene and regulation of vitamin D-dependent expression. *Proc. Natl. Acad. Sci. U.S.A.* **86,** 1143–1147 CrossRef Medline
76. Iso, T., Sartorelli, V., Chung, G., Shichinohe, T., Kedes, L., and Hamamori, Y. (2001) HERP, a new primary target of Notch regulated by ligand binding. *Mol. Cell. Biol.* **21,** 6071–6079 CrossRef Medline
77. Nakagawa, O., Nakagawa, M., Richardson, J. A., Olson, E. N., and Srivastava, D. (1999) HRT1, HRT2, and HRT3: a new subclass of bHLH transcription factors marking specific cardiac, somitic, and pharyngeal arch segments. *Dev. Biol.* **216,** 72–84 CrossRef Medline
78. Gibson, D. G., Young, L., Chuang, R. Y., Venter, J. C., Hutchison C. A., 3rd, and Smith, H. O. (2009) Enzymatic assembly of DNA molecules up to several hundred kilobases. *Nat. Methods* **6,** 343–345 CrossRef Medline
79. Kouadjo, K. E., Nishida, Y., Cadrin-Girard, J. F., Yoshioka, M., and St-Amand, J. (2007) Housekeeping and tissue-specific genes in mouse tissues. *BMC Genomics* **8,** 127 CrossRef Medline
80. Sander, J. D., Zaback, P., Joung, J. K., Voytas, D. F., and Dobbs, D. (2007) Zinc Finger Targeter (ZiFiT): an engineered zinc finger/target site design tool. *Nucleic Acids Res.* **35,** W599–W605 CrossRef Medline
81. Sander, J. D., Maeder, M. L., Reyon, D., Voytas, D. F., Joung, J. K., and Dobbs, D. (2010) ZiFiT (Zinc Finger Targeter): an updated zinc finger engineering tool. *Nucleic Acids Res.* **38,** W462–W468 CrossRef Medline